A biosensor for MAPK-dependent Lin28 signaling

Laurel M. Oldach[a], Kirill Gorshkov[a,b], William T. Mills, IV[c], Jin Zhang[a,d,*], and Mollie K. Meffert[c,e,*]
[a]Department of Pharmacology and Molecular Sciences, [c]Department of Biological Chemistry, and [e]Solomon H. Snyder Department of Neuroscience, Johns Hopkins University School of Medicine, Baltimore, MD 21205; [b]Therapeutics for Rare and Neglected Diseases Program, National Center for Advancing Translational Sciences, National Institutes of Health, Rockville, MD 20850; [d]Department of Pharmacology, University of California, San Diego, La Jolla, CA 92093

ABSTRACT **Intracellular levels of the RNA-binding protein and pluripotency factor, Lin28a, are tightly controlled to govern cellular and organismal growth. Lin28a is extensively regulated at the posttranscriptional level, and can undergo mitogen-activated protein kinase (MAPK)–mediated elevation from low basal levels in differentiated cells by phosphorylation-dependent stabilizing interaction with the RNA-silencing factor HIV TAR RNA-binding protein (TRBP). However, molecular and spatiotemporal details of this critical control mechanism remained unknown. In this work, we dissect the interacting regions of Lin28a and TRBP proteins and develop biosensors to visualize this interaction. We identify truncated domains of Lin28a and of TRBP that are sufficient to support coassociation and mutual elevation of protein levels, and a requirement for MAPK-dependent phosphorylation of TRBP at putative Erk-target serine 152, as well as Lin28a serine 200 phosphorylation, in mediating the increase of Lin28a protein by TRBP. The phosphorylation-dependent association of Lin28a and TRBP truncated constructs is leveraged to develop fluorescence resonance energy transfer (FRET)-based sensors for dynamic monitoring of Lin28a and TRBP interaction. We demonstrate the response of bimolecular and unimolecular FRET sensors to growth factor stimulation in living cells, with coimaging of Erk activation to achieve further understanding of the role of MAPK signaling in Lin28a regulation.**

Monitoring Editor
Alex Dunn
Stanford University

Received: Aug 8, 2017
Revised: Feb 26, 2018
Accepted: Mar 7, 2018

INTRODUCTION

Lin28a is a pluripotency-associated RNA-binding protein that exerts posttranscriptional effects to govern many developmental and cellular signaling pathways (Jiang and Baltimore, 2016). Lin28a promotes progrowth gene expression in part by repressing maturation of the Let-7 family of microRNAs (miRNAs), and undergoes reciprocal translational repression by Let-7 miRNAs (Rybak *et al.*, 2008). Lin28a also controls gene expression through regulation of mRNA translation (Cho *et al.*, 2012). Appropriate control of Lin28a protein levels is necessary for correct organismal development. Mice deficient in Lin28a suffer perinatal lethality (Shinoda *et al.*, 2013). Conversely, Lin28a overexpression can lead to abnormal growth and metabolic phenotypes (Zhu *et al.*, 2010, 2011; Shyh-Chang *et al.*, 2013), and Lin28a is up-regulated in numerous human cancers (Viswanathan *et al.*, 2009; Shyh-Chang and Daley, 2013). Despite a growing appreciation for the necessity of tight control of Lin28a in producing appropriate gene expression programs, the signaling that regulates dynamic changes in Lin28a protein levels remains incompletely understood.

Recently, we reported rapid signal-dependent induction of Lin28a through posttranslational regulation of Lin28a protein stability. MAPK pathway activation was shown to enhance phosphorylation and binding of the Dicer cofactor, TRBP (TAR RNA-binding protein), as well as Dicer itself, to Lin28a in a stabilizing interaction

This article was published online ahead of print in MBoC in Press (http://www.molbiolcell.org/cgi/doi/10.1091/mbc.E17-08-0500) on March 22, 2018.

M.K.M. and J.Z. conceived of the project and supervised its execution. L.O. planned and carried out experiments and analyses in Figures 1–4 and 5, A, B, E, and F. K.G. carried out experiments in Figure 5, C, D, and G, and Supplemental Figure S4, A and B, and assisted with image preparation. W.M. performed cloning in Supplemental Figure S4C. L.O., M.K.M., and J.Z. wrote the manuscript.

*Address correspondence to: Jin Zhang (jzhang32@ucsd.edu), Mollie K. Meffert (mkm@jhmi.edu).

Abbreviations used: dsRBM, double-stranded RNA-binding motif; EKAR, Erk kinase activity reporter; FL-Lin28a, Flag-tagged Lin28a; FSP/FXP, amino acid sequence of Erk docking motif; MAPK, mitogen-activated protein kinase; miRNA, microRNA; TRBP, TAR RNA-binding protein.

(Amen *et al.*, 2017). This complex exerts selectivity in miRNA biogenesis, allowing Lin28a to reduce the level of Let-7 miRNAs while Dicer enhances maturation of many miRNAs not targeted by Lin28 (Huang and Ruiz *et al.*, 2012). A Lin28a/TRBP/Dicer protein complex was described initially in cultured neurons, but mitogen-activated protein kinase (MAPK)–dependent TRBP phosphorylation and Lin28a elevation were also observed downstream from trophic factors in other primary cell types, indicating a widespread role for this interaction in regulating growth responses (Amen *et al.*, 2017). However, molecular details of the Lin28a/TRBP interaction, including its time scale and spatial distribution in cells, were relatively unexplored. In this work, we characterize the biology of Lin28a and TRBP interacting domains. We identifiy a TRBP phosphorylation site crucial for signal-responsive interaction with Lin28a and leverage this characterization to develop a genetically encoded fluorescent biosensor for Lin28a/TRBP binding, allowing examination of the magnitude and spatiotemporal visualization of Lin28a/TRBP binding in living cells.

RESULTS AND DISCUSSION

A TRBP truncation sufficient to interact with full-length Lin28a

To investigate TRBP-induced elevation of Lin28a protein levels, we first identified the region of TRBP required for this response. Truncation mutants of TRBP, TRBP-A (1–105), TRBP-B (98–234), TRBP-AB (1–234), and TRBP-C (228–366; Figure 1A), developed by the Gatignol laboratory (Daher *et al.*, 2009), were tagged with the myc epitope. When coexpressed in HEK 293T cells with flag-tagged lin28a (FL-Lin28a), TRBP-A and TRBP-B both elevated FL-Lin28a, while TRBP-C had no effect (Figure 1, B and C). Expression of TRBP-C was low, even with high DNA transfections (Supplemental Figure S1A). Dose titration showed that elevation of FL-Lin28a protein by TRBP-A and TRBP-B was most readily detected at low FL-Lin28a expression levels (Supplemental Figure S1, B and C). Expressed TRBP-B could also elevate levels of endogenous TRBP protein (Figure 1D), in line with a previous demonstration that dsRNA binding motifs (dsRBMs) in these two truncations mediate TRBP dimerization (Kok *et al.*, 2007). To distinguish effects on Lin28a elevation due to the TRBP truncation alone from effects that might result from heterodimerization of a TRBP truncation with endogenous TRBP, we next carried out experiments in TRBP knockout cells.

Coexpression of TRBP-A and TRBP-B with FL-Lin28a in mouse tail epithelial fibroblast cells (TEFs) lacking endogenous murine TRBP (*Tarbp2* KO; Daher *et al.*, 2009) revealed that TRBP-B, but not TRBP-A, could elevate FL-Lin28a levels; TRBP-B increased FL-Lin28a comparably to full-length TRBP expression (Figure 1, E–G). Across a range of expression levels in TRBP KO TEFs, full-length TRBP and the TRBP-B truncation produced approximately linear FL-Lin28a protein elevations, while no increase in FL-Lin28a was observed with TRBP-A (Figure 1G). These results strongly suggested that TRBP-B retained the capacity to interact with Lin28a, while effects of TRBP-A were absent when endogenous full-length TRBP could not be recruited.

In previous work, we demonstrated that full-length TRBP can directly bind Lin28a in a stabilizing complex (Amen *et al.*, 2017). Thus, we next compared the association of truncations TRBP-A, TRBP-B, and TRBP-AB with FL-Lin28a. Immunoprecipitation of FL-Lin28a from 293T cells showed that TRBP-AB coimmunoprecipitated with FL-Lin28a, as did TRBP-B more weakly, while TRBP-A did not coimmunoprecipitate with FL-Lin28a (Figure 1H). Because TRBP-B expression is sufficient to elevate Lin28a levels (Figure 1, B–G), we speculate that reduced stability during the process of immunoprecipitation may contribute to relatively modest coimmunoprecipitation with Lin28a (Figure 1H). Collectively, these results are consistent with binding and increase of Lin28a by the TRBP-B segment of TRBP, but not by the N-terminal or C-terminal segments TRBP-A and C.

TRBP phosphorylation at S152 potentiates Lin28a elevation

TRBP phosphorylation has been shown to increase its stability (Chen *et al.*, 2015) and enhance binding to Dicer and other binding partners (Paroo *et al.*, 2009; Kim *et al.*, 2014). In addition, we previously showed that a phosphomimic TRBP mutant, with four serines mutated to aspartates, exhibited enhanced binding to Lin28a in purified protein interactions (Amen *et al.*, 2017). These findings implicated MAPK pathway-mediated phosphorylation of TRBP in Lin28a binding, without indicating which of the four serine residues was involved. We identified an "FXF" putative Erk docking motif (Gonzalez *et al.*, 1991) within TRBP-B, beginning at aa 112. Two of the serines mutated in the full-length phosphomimic construct, S142 and S152, are present in TRBP-B; both serines are candidates for proline-directed kinase phosphorylation, but S152 is a closer match to an Erk phosphorylation consensus sequence (Figure 2A, PXSP; Jacobs *et al.*, 1999).

Immunoblot of lysates from 293T cells expressing myc-TRBP-B revealed a multibanding pattern between 20 and 25 kDa when probed with an antibody raised and purified against phospho-S152 TRBP (Supplemental Figure S2A). Consistently, exposure of myc-TRBP-B lysates to lambda phosphatase treatment collapsed the myc-reactive bands to a singlet at the expected molecular weight of TRBP-B (Figure 2B). Phorbol 12-myristate 13-acetate (PMA) can increase TRBP phosphorylation through the MAPK signaling cascade (Paroo *et al.*, 2009). Treating 293T cells expressing myc-TRBP-B with PMA led to an increase in phospho-S152 TRBP immunoreactivity, which was reduced in lysates from cells treated with MAPK/Erk kinase (MEK) inhibitor U0126 (Figure 2C and additional representative blot Supplemental Figure S2B). We conclude that TRBP-B can be phosphorylated within living cells in a MEK-dependent manner. To evaluate the role of this TRBP phosphorylation site in producing Lin28a elevation, we immunoblotted lysates from 293T cells which were coexpressing FL-Lin28a and myc-TRBP-B, and treated with either vehicle control, PMA, or PMA plus U0126. Immunoblot showed that FL-Lin28a protein levels were increased by myc-TRBP-B expression, and that PMA treatment further enhanced Lin28a elevation in a manner blocked by U0126 (Figure 2, C and D).

We next conducted experiments in TRBP KO TEFs to specifically evaluate the role of the putative Erk phosphorylation site TRBP S152 in conferring stimulus-mediated Lin28a elevation by TRBP-B. A phosphomutant myc-TRBP-B with S152 mutated to alanine was generated and we observed that reactivity of the TRBP-B band with anti-phospho-TRBP antibody was abolished in cells expressing TRBP-B S152A (Figure 2E and Supplemental Figure S2C). In TRBP KO TEFs coexpressing FL-Lin28a and either myc-TRBP-B or phosphomutant myc-TRBP-B-S152A (at similar levels; Supplemental Figure S2D), TRBP-B or TRBP-B S152A expression could each produce some basal Lin28a elevation, but cells expressing TRBP-B S152A were unable to respond to PMA (Figure 2F). PMA produced a modest Lin28a induction in the absence of TRBP-B expression, an effect which might be due to direct Lin28a phosphorylation (Liu *et al.*, 2017; Tsanov *et al.*, 2017) or an alternative unknown interacting protein. In addition, we observed that purified GST-TRBP-B protein could specifically coassociate with purified Lin28a, compared with GST alone, and that this association was decreased by the phosphomutation TRBP-B S152A (Supplemental Figure S2E). Decreased binding of Lin28a by TRBP-B SA, in comparison to wild-type TRPB-B, may be due to reduced phosphorylation in bacteria (Macek and Mijakovic, 2011; Pereira *et al.*, 2011; Cousin *et al.*, 2013) or to

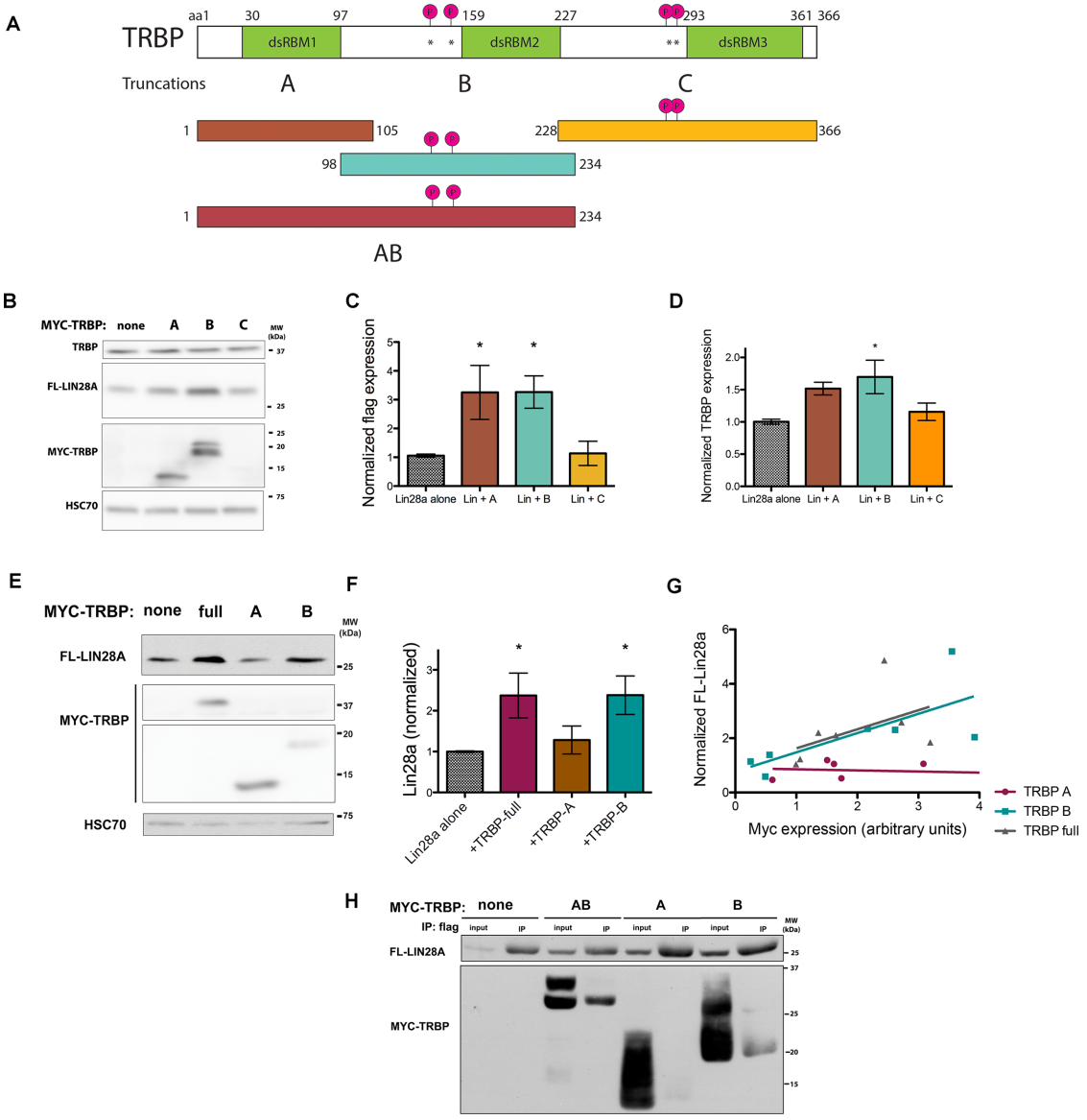

FIGURE 1: A TRBP truncation sufficient to bind and elevate Lin28a levels. (A) Domain map of TRBP, with truncations TRBP-A, B, C and TRBP-AB. Phosphorylation sites (pink) as described (Paroo *et al.*, 2009), at serine residues 142, 152, 283, and 286. (B, C) TRBP-A and B stabilize FL-Lin28a in 293T cells. Representative immunoblot (B) of lysates of 293T cells expressing Lin28a alone or coexpressing Lin28a with TRBP truncations, and quantified data normalized to HSC70 loading control (C; $n = 7–14$). (D) Increase in endogenous TRBP level, normalized to HSC70, quantified from immunoblots of lysates of 293T cells expressing Lin28a alone or coexpressing Lin28a with TRBP truncations ($n = 5–8$). (E, F) Full-length TRBP (TRBP full) and TRBP-B, but not TRBP-A, elevate Lin28a levels from baseline in Tarbp2–/– MEF cells. Representative immunoblot (E) and quantification (F) of FL-Lin28a normalized to HSC70 and plotted relative to the Lin28a alone condition set as 1.0 ($n = 9$). (G) Scatterplot of the FL-Lin28a protein levels relative to the coexpression level of full-length TRBP, TRBP-A, or TRBP-B proteins in Tarbp2–/– cells. FL-Lin28a levels were positively correlated with increasing expression TRBP full and TRBP-B. The regression line for TRBP full has a correlation coefficient (r) of 0.51 ($p = 0.114$ for deviation from zero slope). One statistically significant outlier was removed (*Materials and Methods*). Myc TRBP-A regression $r = 0.06$ ($p = 0.638$) and Myc TRBP-B regression $r = 0.62$ ($p = 0.06$). (H) Coimmunoprecipitation of FL-Lin28a with myc-TRBP-AB and B, but not TBRP-A. (A–F) *, $p < 0.05$, ANOVA.

the absence of the hydroxyl group on residue 152. This result is consistent with previous work showing that a purified recombinant full-length phosphomimic TRBP protein interacts more strongly in vitro with Lin28a in comparison to recombinant wild-type TRBP (Amen *et al.*, 2017). Collectively, these experiments indicate that the TRBP-B region is sufficient to bind and elevate Lin28a protein levels, and support a role for TRBP S152 in transducing MAPK pathway activation through TRBP to regulate Lin28a.

Lin28a-3 interacts with full-length TRBP and TRBP-B

To address which region of Lin28a protein interacted with TRBP, we generated three domain-based truncations of Lin28a (Figure 3A). Because Lin28b, a paralog with 86% amino acid identity between Lin28A amino acids 19 and 177, fails to bind to TRBP (Amen *et al.*, 2017), we reasoned that amino acid sequences unique to Lin28a at the amino or the carboxy terminus of the protein might participate in TRBP interaction. Truncations were designed to correspond to

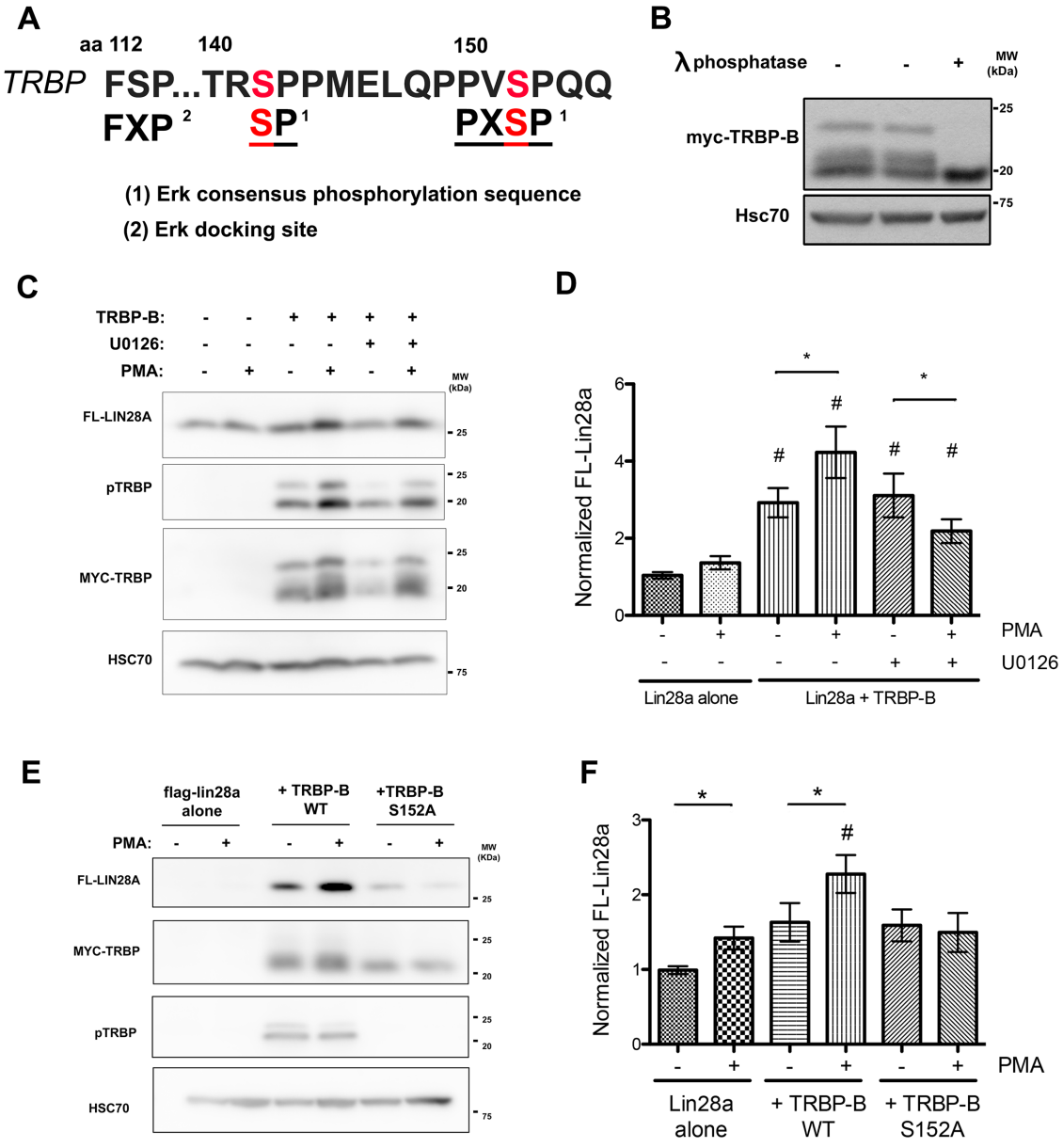

FIGURE 2: TRBP-B phosphorylation at S152 enhances binding to Lin28a. (A) Putative ERK substrate sequence of TRBP at serine 152, including FSP docking site. Weaker candidate ERK substrate at serine 142. (B) Immunoblot from 293T cells expressing TRBP-B shows two or more phosphorylated species exist and can be collapsed by lysate treatment with lambda phosphatase. (C, D) Representative blot and quantitation showing levels of FL-Lin28a, phospho-TRBP, and myc-TRBP-B proteins from 293T cells pretreated with U0126 (20 uM), with or without PMA treatment (50 ng/ml; $n = 15$). (E, F) Representative blot and quantitation showing effect of PMA on FL-Lin28a level in Tarbp2−/− MEF cells coexpressing TRBP-WT or S152A and treated with PMA ($n = 8$). (D, F) #, $p < 0.05$, ANOVA; *, $p < 0.05$, paired t test.

functional domains of Lin28a revealed by its crystal structure (Nam *et al.*, 2011; Mayr *et al.*, 2012). Lin28a-1, aa 1–112, included the structurally uncharacterized amino terminus and the cold-shock domain (CSD). Lin28a-2, aa 75–154, encompassed half of the CSD, extending to the end of the CCHC Zn knuckles. Lin28a-3 began at the amino terminus of the CCHC, extending to the structurally uncharacterized carboxy terminus of the protein (Figure 3A).

Full-length FL-Lin28a and FL-Lin28a-3 levels were each elevated above baseline by myc TRBP coexpression in 293T cells (Figure 3, B and C). In some experimental replicates, we observed mild increases in FL-Lin28a-1 by TRBP. We tested whether, like full-length FL-Lin28a, either FL-Lin28a-1 or FL-Lin28a-3 could be elevated by treatment with PMA (24 h) in 293T cells coexpressing TRBP-B. FL-Lin28a-1 levels were not significantly changed either by coexpression of TRBP-B alone or by TRBP-B plus PMA stimulation, while FL-Lin28a-3 levels were robustly increased by TRBP-B coexpression and further enhanced by PMA treatment (Figure 3, E and F).

In addition to TRBP phosphorylation, Lin28a has also been reported to undergo MAPK-dependent phosphorylation at serine 200, which can regulate its stability (Liu *et al.*, 2017; Tsanov *et al.*, 2017). To evaluate the participation of Lin28a-3 phosphorylation, compared with TRBP-B phosphorylation (Figure 2, E and F), in Lin28a-3 protein up-regulation, we assessed the fold stabilization of wild-type and phosphomutant FL-Lin28a-3 (Lin28a-3 S200A) by immunoblot of

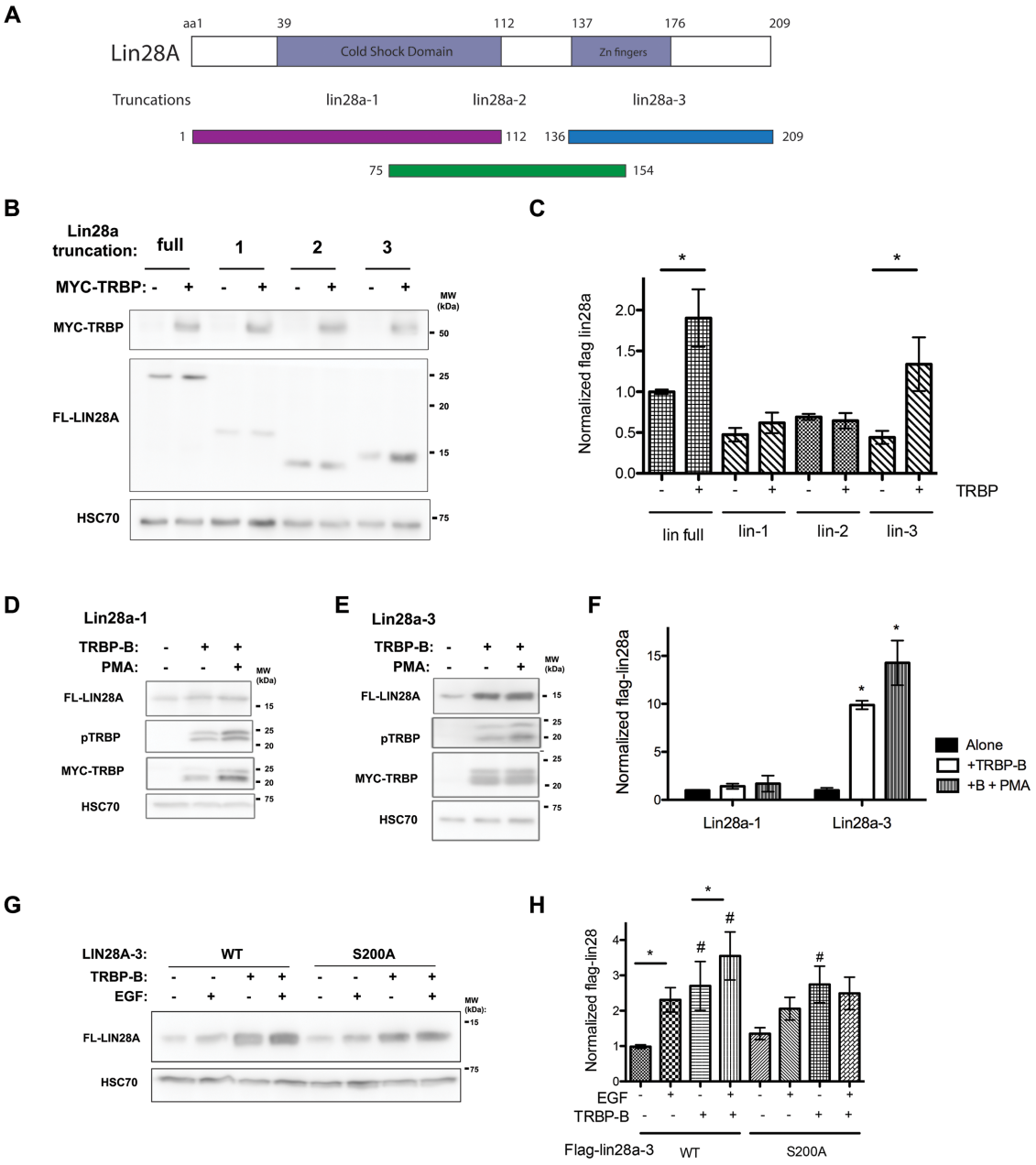

FIGURE 3: A C-terminal Lin28a truncation sufficient to respond to TRBP and TRBP-B. (A) Domain map of Lin28a, with truncations Lin28a-1, 2, and 3. (B, C) Coexpression of FL-Lin28a and truncations with full-length TRBP in 293T cells increases Lin28a and Lin28a-3. (*, $p < 0.05$, ANOVA, $n = 4$). (D–F) Effect of coexpression of TRBP-B and treatment with PMA on protein level of FL-Lin28a-1 (D) and FL-Lin28a-3 (E) (*, $p < 0.01$, two-way ANOVA, $n = 3$–5). (G, H) Effect of coexpression of TRBP-B and treatment with EGF on protein level of WT or S200A FL-Lin28a-3 (#, $p < 0.01$, ANOVA; *, $p < 0.05$, paired t test; $n = 9$).

293T cell lysates in the presence or absence of TRBP-B coexpression or epidermal growth factor (EGF) treatment (Figure 3, G and H). Levels of wild-type FL-Lin28a-3 protein were significantly elevated by coexpression with TRBP-B, and this effect was further enhanced by 293T stimulation with EGF (one-way analysis of variance [ANOVA] compared with wild-type Lin28a-3 alone). In contrast, levels of FL-Lin28a-3 S200A protein could be increased by TRBP-B coexpression but were not further affected by EGF treatment (one-way ANOVA); pairwise t tests revealed that there was a significant effect of EGF treatment with wild-type Lin28a-3 (Figure 3H). These results indicate that phosphorylation of both TRBP S152 and of Lin28a S200 participate in the induction of Lin28a protein levels by TRBP expression and stimuli producing MAPK pathway activation.

Lin28a-3 interacts with TRBP-B in a phosphorylation-inducible manner

The identification of Lin28a-3 and TRBP-B as interacting truncations which reproduce the induction observed with full-length TRBP and Lin28a proteins, presented an opportunity to create a physiological sensor for this pathway. We assayed the efficiency of fluorescence resonance energy transfer (FRET) between TRBP constructs tagged with the CFP variant, Cerulean, and Lin28a constructs tagged with a

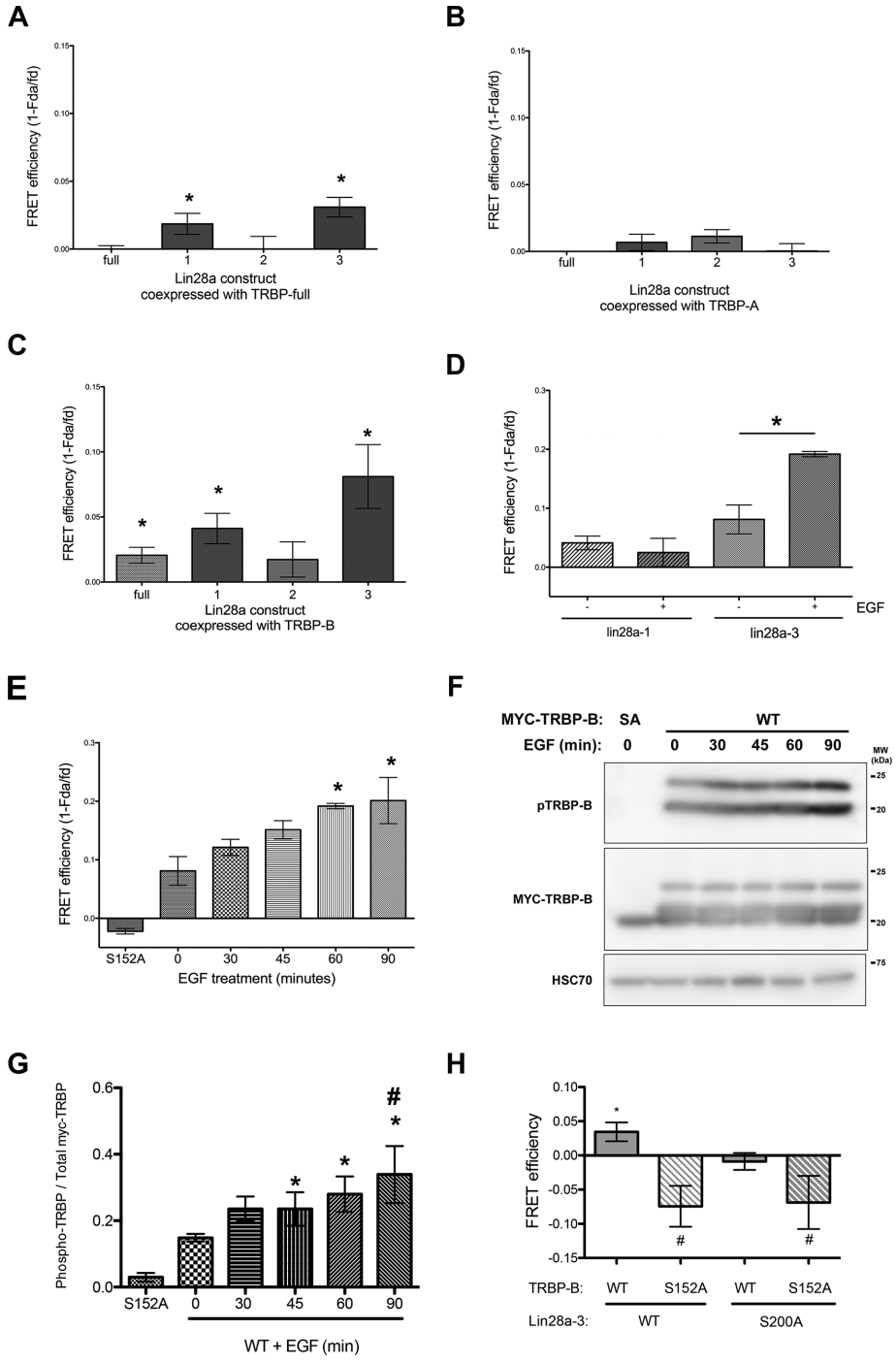

FIGURE 4: Lin28a-3 interacts with TRBP-B in a phosphorylation-inducible manner. (A) FRET efficiency of C-terminal cpVenusE172-tagged Lin28a and truncations with full-length N-terminal Cerulean3-tagged TRBP. (B, C) FRET efficiency of Lin28a and truncations with TRBP-A and B. (A–C) *, $p < 0.05$ vs. 0, *t* test. (D) FRET efficiency of Lin28a-1 and 3 with TRBP-B after treatment with 100 ng/ml EGF for 60 min. (E) FRET efficiency of Lin28a-3 with TRBP-B after EGF treatment. "S152A" indicates efficiency of Lin28a-3 with phosphomutant TRBP-S152A (D, E; * $p < 0.05$ vs. untreated, ANOVA). (A–E) $n = 15$–75 cells per column from at least two dishes. (F, G) Increase in phospho-TRBP-B, measured by immunoblot, after EGF treatment. (#, $p < 0.05$, ANOVA; *, $p < 0.05$, paired *t* test; $n = 6$). (H) FRET efficiency, measured with a different instrument, for Lin28a-3 WT and S200A with TRBP-B WT and S152A (*, $p < 0.05$ vs. 0, *t* test; #, $p < 0.05$ vs. WT/WT pair, ANOVA).

circular permutation of the Venus YFP, cpVenusE172. FRET was measured in living 293T cells by bleaching the FRET acceptor, YFP, and measuring dequenching of the donor, CFP. As a benchmark for high FRET efficiency in our imaging system, we used a FRET sensor for calmodulin (Supplemental Figure S3A; Romoser *et al.*, 1997). We confirmed YFP bleaching to 75% or greater reduction of signal in each cell (Supplemental Figure S3, B–D).

We tested the effects of coexpressing CFP-tagged full-length TRBP and TRBP truncations, TRBP-A and TRBP-B, with a panel of YFP-tagged Lin28a constructs in 293T cells. When coexpressed with full-length TRBP, both Lin28a-1 and Lin28a-3 showed positive FRET efficiency, indicative of significant interaction (Figure 4A). In congruence with our previous findings, FRET efficiency of Lin28a-3-YFP with CFP-TRBP was highest, followed by Lin28a-1-YFP, with no FRET between Lin28a-2-YFP and CFP-TRBP (Figure 4A). Consistent with its failure to elevate Lin28a protein levels, TRBP-A displayed no FRET-detectable interaction with any Lin28a-YFP truncation (Figure 4B). In contrast, TRBP-B showed significant CFP recovery when coexpressed with Lin28a-1-YFP, Lin28a-3-YFP, or full-length Lin28a-YFP (Figure 4C). CFP-TRBP-AB showed FRET intermediate between full-length and TRBP-B (Supplemental Figure S3, E and F), and was not pursued further as the more effective and shorter TRBP-B truncation was also less likely to mimic or preclude endogenous TRBP function. We noted that full-length Lin28a, known to be capable of direct binding to TRBP (Amen *et al.*, 2017; Supplemental Figure S2E), did not show significant CFP recovery after photobleaching (Figure 4A). This result is consistent with a risk of false-negative results from FRET analyses based on fluorophore orientation (Miyawaki, 2011). On the basis of these results, we concluded that TRBP-B can interact with Lin28a-3, and also to a lesser degree with Lin28a-1. Further, observed FRET efficiency of the Lin28a-3-YFP and CFP-TRBP-B was higher than between full-length Lin28a and TRBP, indicating that the truncated constructs produce a preferred conformation for a FRET biosensor.

To determine whether TRBP binding by Lin28a-1 or Lin28a-3 could be increased by phosphorylation, we treated 293T cells expressing CFP-TRBP-B and either Lin28a-1-YFP or Lin28a-3-YFP with either EGF (a MAPK pathway activator) or vehicle and measured donor dequenching 60 min after treatment (Figure 4D). FRET between CFP-TRBP-B and Lin28a-3-YFP increased significantly after EGF treatment (Figure 4D), consistent with the stimulus-dependent increase in protein levels observed in Figure 3, E and F. In contrast, EGF treatment did not alter FRET efficiency of Lin28a-1-YFP and CFP-TRBP-B. Notably, there was no detectable FRET between Lin28a-3-YFP and

the S152A phosphomutant CFP-TRBP-B S152A, indicating a critical role for this serine residue in interaction of the Lin28a/TRBP FRET sensor (Figure 4E). In cells treated with EGF for variable times before acceptor bleaching, CFP-TRBP-B and Lin28a-3-YFP demonstrated a time-dependent increase in FRET with a maximal plateau by 60–90 min (Figure 4E). This corresponded with a similar time-dependent increase in the ratio of phosphorylated TRBP-B to total myc-TRBP-B observed by immunoblot after EGF treatment (Figure 4, F and G).

The importance of phosphorylation for TRBP-B and Lin28a-3 interactions was further evaluated by testing the effects of phosphomutant constructs, CFP-TRBP-B S152A and Lin28a-3 S200A-YFP, on FRET efficiency. We conducted a multicomponent FRET comparison assessing basal FRET with the following pairs: TRBP-BWT/Lin28a-3WT, TRBP-BS152A/Lin28a-3WT, TRBP-BWT/Lin28a-3S200A, and TRBP-BS152A/Lin28a-3S200A (Figure 4H). Significant positive FRET was observed only with the wild-type (TRBP-BWT/Lin28a-3WT) pair. FRET efficiency of both FRET pairs containing phosphomutant TRBP-B (TRBP-BS152A) were significantly reduced from the wild-type FRET pair. A FRET pair containing wild-type TRBP-B and phosphomutant Lin28a-3 (Lin28a-3 S200A) failed to show positive FRET, but was also not significantly different from zero or from the wild-type FRET pair. We note that a necessitated change in imaging system (Figure 4H compared with the system used in Figure 4, A–E) contributed to mild CFP photodamage that underlies reduced basal FRET values in Figure 4H but does not impact the validity of comparisons, which are made within the experiment. Collectively, results from our experiments using phosphomutants of TRBP-B (Figures 2, E and F, and 4, E–H) and Lin28a-3 (Figures 3G and 4H) indicate that phosphorylation of both S152 on TRBP and of S200 on Lin28a can contribute to MAPK-dependent co-up-regulation of these proteins, although the impact of TRBP S152 phosphorylation may marginally predominate in our assay system.

Optimization and validation of a sensor for Lin28a/TRBP binding

On the basis of the observation that FRET between TRBP-B and Lin28a-3 was increased within 90 min by EGF, and absent with phosphomutant TRBP-B, we performed time-lapse experiments to characterize the stimulation kinetics in more detail. We expressed CFP-TRBP-B and Lin28a-3-YFP in 293T cells and calculated the ratio of sensitized YFP fluorescence emission, determined using the NFRET formula, to CFP fluorescence (Xia and Liu, 2001). Baseline emission ratios were measured in individual cells for 10 min, followed by imaging for 35 min after EGF treatment. EGF induced a modest average change in NFRET (Figure 5, A and B; "Cer/E172"), indicating that further optimization might generate a more useful sensor for TRBP-Lin28a interaction. To enhance the dynamic range of the sensor, we tested a panel of FRET pairs, a strategy that has improved previous sensors (Figure 5A; Zhou *et al.*, 2015). Optimization resulted in a marked improvement, with the new FRET pair showing higher average response to EGF (Figure 5B; "Cer3/L194"). We tested the dependence of the Cer3/L194 Lin28a/TRBP FRET sensor on MEK activity. Consistent with previous Lin28a/TRBP interactions, MEK inhibition with U0126 (30 min) blocked EGF-induced NFRET increases, whereas 293T cells pretreated with vehicle retained an EGF-stimulated increase in NFRET (Figure 5C).

To investigate the temporal relationship between Erk activation and Lin28a/TRBP binding, we coexpressed an intensitometric Erk activity sensor (EKAR) based on dimerization-dependent RFP (Ding *et al.*, 2015) with the optimized Lin28a/TRBP sensor. The spectral separation between Cerulean3/Venus and RFP permitted us to monitor signal-induced changes in single cells at these two different steps within the EGF response pathway. Representative images of cells before and for 80 min after EGF treatment are shown in Figure 5D. Consistent with our earlier demonstration that S152A TRBP-B failed to show detectable FRET with Lin28a-3, we observed that the NFRET/CFP ratio between the phosphomutant and Lin28a-3 did not increase after EGF treatment, although EKAR activity indicates rapidly peaking Erk activation (Figure 5E). In contrast, 293T cells expressing the sensor using WT-TRBP-B demonstrate NFRET response to EGF (Figure 5F). Erk activity reached a plateau within 15 min of EGF on average, and remained at peak activity for the duration of imaging (Figure 5F, red curve). The NFRET signal from the optimized Lin28a/TRBP sensor increased more gradually, showing slower kinetics than Erk activity (Figure 5F, black curve). This slower Lin28a/TRBP FRET response compared with EKAR was reproduced in cells treated with PMA (Supplemental Figure S5, A and B). We noted that cells with stronger EKAR response also showed greater increases in Lin28a/TRBP NFRET, and analyzed the correlation between response magnitude in the two signals. Comparing the increase in EKAR intensity at 30 min of EGF, to the increase in NFRET at the same time point, we observed a positive correlation in these two readouts (Figure 5G). We conclude that this sensor is a reliable tool for imaging ongoing changes in Lin28a/TRBP binding in real time within cells.

Compared with bimolecular FRET sensors, unimolecular FRET-based biosensors offer advantages in that they do not require equivalent coexpression of constructs and, due to tethering, they produce virtually complete colocalization of the fluorescent biosensor components. Prompted by the efficacy of the bimolecular Lin28a/TRBP sensor, we developed a unimolecular version by introducing a linker domain between Cer3-TRBP-B and Lin28a-3-YFP (Figure 4C). After 30 min of EGF treatment (100 ng/ml) in 293T cells, the expressed unimolecular sensor exhibited a twofold increase in FRET efficiency (Supplemental Figure S4D), compared with a 1.5-fold increase over baseline FRET efficiency in the bimolecular sensor at this same 30 min time point (Figure 4E). As expected, CFP/YFP colocalization was also improved in the unimolecular compared with the bimolecular sensor (Supplemental Figure S4E). In future studies, this optimized unimolecular Lin28a/TRBP biosensor may also facilitate tagging for targeting to discrete subcellular locations to visualize variability and temporal dynamics in signal-dependent regulation of miRNA biogenesis.

Signal-responsive regulation of miRNA biogenesis factors allows rapid changes in miRNA content in response to dynamic cellular and environmental contexts (Baek *et al.*, 2008; Selbach *et al.*, 2008). In this work, we dissected a MAPK-dependent mechanism for enhancing the interaction between two miRNA-binding proteins, Lin28a and TRBP, which can selectively modulate mature miRNA production. We found that expression of a midregion of TRBP (TRBP-B, amino acids 98–234), containing the second dsRBM, was sufficient to elevate levels of Lin28a protein in a manner indistinguishable from full-length TRBP, whereas a TRBP truncation lacking this midregion failed to increase Lin28a (Figure 1, E–G). TRBP-B, as well as a larger TRBP truncation containing the same middle region (TRBP-AB), could each associate with Lin28a in cellular lysates (Figure 1H), while a truncation lacking this region did not. Interestingly, another TRBP-binding protein, Dicer, has been shown to associate with the carboxy terminus of TRBP by crystal structure (using TRBP amino acids 258–366 only; Wilson *et al.*, 2015) and by biochemical mapping (TRBP amino acids 298–366; Daniels *et al.*, 2009); this may perhaps enable the simultaneous association by different regions of full-length TRBP with both Dicer and Lin28a as has been

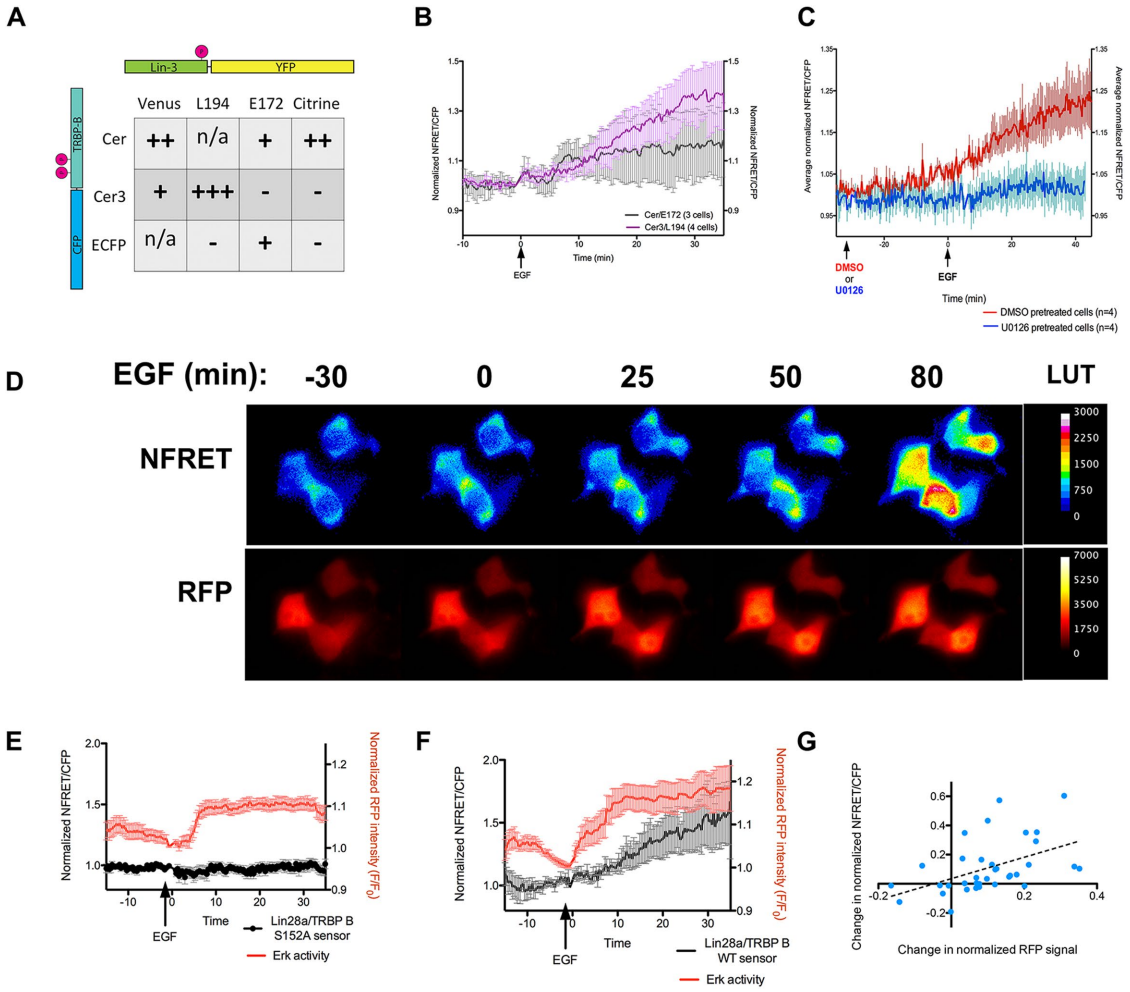

FIGURE 5: Optimization of a sensor for phosphorylation-induced Lin28a/TRBP binding. (A) Qualitative assessment of Lin28a/TRBP FRET pairs, scored based on flat baseline and magnitude of response (n = 2–6 dishes/pair). (B) Comparison of NFRET ratio change, normalized to T0, between representative 293T cells expressing sensor with original FRET pair ("Cer/E172") or optimized sensor ("Cer3/L194") after EGF treatment. (C) Optimized sensor FRET response to EGF in 293T cells pretreated with vehicle (red) or U0126 (blue; n = 4 cells per condition). (D) Pseudocolor image series of Cer3/L194 sensor signal ("NFRET") and EKAR sensor intensity ("RFP") in 293T cells pretreated with dimethyl sulfoxide and then treated with EGF. (E, F) Representative curves showing change in NFRET (black) coimaged with increase in Erk activity (red) in response to EGF in cells expressing S152A sensor (E; n = 7) or WT sensor (F; n = 6). (G) Regression analysis of EKAR intensity change and NFRET intensity change, measured 30 min after EGF treatment (n = 35 cells from seven dishes). Regression line r = 0.23 (p = 0.004).

previously demonstrated (Amen *et al.*, 2017). TRBP binding increases the stability of Dicer (Paroo *et al.*, 2009; Wilson *et al.*, 2015), and TRBP phosphorylation at serines 142, 152, 283, and 286 has been previously reported to increase TRBP stability and elevate levels of both TRBP and Dicer (Paroo *et al.*, 2009).

Of the three domain-based Lin28a truncations tested, only Lin28a-3, which begins at the CCHC zinc knuckles and terminates at the carboxy terminus of the protein (amino acids 136–209), exhibited elevated protein levels when coexpressed with full-length TRBP or with TRBP-B (Figure 3, B and C), and signal-induced elevation in cells coexpressing TRBP-B (Figure 3, D–H). While FRET pairs containing either the N-terminal Lin28a truncation (Lin28a-1) or Lin28a-3 with TRBP-B exhibited FRET, FRET efficiency with Lin28a-3 was not only strongest at baseline but also capable of stimulus-mediated increase (Figure 4, A–E). Low basal FRET between Lin28a-1 and TRBP-B could occur due to a secondary interface between the two proteins not detected by an immunoprecipitation approach. These data suggest that the C-terminal Lin28a-3 truncation contains a minimal unit for signal-inducible binding to TRBP. Our finding that the signal-inducible binding region of Lin28a includes regions of lower homology with vertebrate paralog Lin28b, such as the C-terminal 20 amino acids of Lin28a-3, is consistent with previous work showing that full-length Lin28a can coassociate with TRBP, whereas the highly homologous Lin28b does not (Amen *et al.*, 2017).

Collectively, our data support a model in which phosphorylation of both Lin28a and TRBP contribute to their signal-induced interaction. We identified a role for TRBP phosphorylation at serine 152, an Erk consensus site proximal to a putative Erk docking site, in enhancing Lin28a interactions after cellular MAPK pathway activation with EGF or PMA. Although phosphomutant TRBP-B S152A remained able to stabilize full-length Lin28a over baseline (Figure 2, D and F), it was unable to participate in signal-enhanced elevation of Lin28a protein or FRET efficiency. These findings highlight a role for TRBP S152 in signal-dependent enhancement of TRBP-Lin28a

interactions and induction of Lin28a protein. The dsRBMs of TRBP, including the motif within TRBP-B, participate in homodimerization and binding to other proteins, most notably PACT and PKR (Daher *et al.*, 2001; Laraki *et al.*, 2008), and could also play a role in basal binding to Lin28a. Binding to RNA has previously been shown to facilitate the interaction of full-length Lin28a and TRBP in cell extracts (Amen *et al.*, 2017), and might enhance intracellular interaction of TRBP-B and Lin28a-3 in the biosensor. In addition to TRBP phosphorylation, we found that phosphorylation of Lin28a-3 participated in potentiating interaction with TRBP-B and elevating Lin28a-3 levels. Lin28a serine 200 phosphorylation has been previously reported to regulate Lin28a stability (Liu *et al.*, 2017; Tsanov *et al.*, 2017). Data from our FRET experiments using S-to-A phosphomutants (Lin28a-3 S200A and TRBP-B S152A) showed that phosphorylation of both TRBP and Lin28a were required for maximal interaction, and phosphomutants of either Lin28a-3 or TRBP-B reduced FRET-detectable interaction. Direct binding of activated ERK to TRBP has been previously reported (Paroo *et al.*, 2009) and the TRBP-B truncation contains a putative ERK docking site (Figure 2A), making it interesting to speculate whether this could participate in recruiting activated ERK to the proximity of a Lin28a/TRBP complex.

The developed Lin28a/TRBP FRET sensor leverages the utility of FRET imaging approaches for probing complex protein/protein interactions to provide spatiotemporal information about specific binding interactions. We observed that FRET signal, indicative of Lin28a and TRBP binding, exhibited slower kinetics relative to Erk phosphorylation readout from the EKAR sensor. We did not find a condition that induced return of the FRET signal to baseline levels, suggesting that signal-induced binding of the sensor may persist despite dephosphorylation, or that the truncation constructs included in the sensor lack a sequence involved in dissociation or dephosphorylation. The TRBP literature implicates multiple proline-dependent MAPKs, chiefly Erk and JNK, in TRBP regulation (Kim *et al.*, 2014; Chen *et al.*, 2015; Warner *et al.*, 2016), including additional residues within TRBP-B. This FRET sensor may be of future use in probing the function of these phosphoregulatory sites, as well as investigation of compartmentalized TRBP and Lin28a interactions in a variety of physiological contexts. For example, both TRBP and Lin28a have roles in protein translation and silencing in the periendoplasmic reticulum region (Cho *et al.* 2012; Stalder *et al.*, 2013). Similarly, the sensor could be used to gain spatiotemporal information regarding TRBP interaction with Lin28a occurring downstream from neurotrophins (Huang and Ruiz *et al.*, 2012; Ruiz *et al.* 2014; Amen *et al.*, 2017), which may exert effects on synaptic plasticity and protein synthesis in a variety of neuronal compartments.

MATERIALS AND METHODS

Cloning

TRBP truncations (as published [Daher *et al.*, 2001]) were N-terminally tagged with myc (MEEQKLISEEDL), or fluorescent proteins Cerulean (Rizzo *et al.*, 2004), Cerulean-3 (Markwardt *et al.*, 2011), or ECFP (Llopis *et al.*, 1998) in a pcDNA3.1+ vector backbone. Lin28a truncations were derived from FL-Lin28a (Amen *et al.* 2017) by PCR and tagged with flag (DLYDDDKD) at the amino terminus or YFP variants Venus (Nagai et al 2002), Citrine (Griesbeck *et al.*, 2001), cpVenus-E172, or cpVenus-L194 (Nagai *et al.* 2004) at the carboxy terminus. Phosphomimic and phosphomutant versions of all TRBP and Lin28a constructs were derived from wild-type versions of these constructs, using a QuickChange kit (Agilent) per manufacturer protocols. A unimolecular sensor was developed using Gibson assembly to fuse Cer3-TRBP-B and Lin3-L194 with a flexible linker from the EKAR sensor (Ding *et al.*, 2015) in a pcDNA 3.1+ backbone. EKAR ratiometric Erk sensor was a gift from Robert Campbell (University of Alberta, Edmonton, Canada) (Addgene; plasmid #60974).

Cell culture

HEK 293T cells were cultured and transfected as described (Amen *et al.*, 2017). When multiple truncations of the same protein were expressed for the same experiment, transfection levels were optimized to equalize affinity tag level in lysates from different truncations. Total DNA transfected was equalized between conditions using empty pcDNA vector. Mouse tail epithelial fibroblast cells (TEFs) lacking endogenous murine TRBP (*Tarbp2* KO; gift of Anne Gatignol, McGill University, Montreal, QC, Canada [Daher *et al.*, 2009]) were cultured in DMEM with 10% fetal bovine serum supplemented with penicillin and streptomycin. Cells were seeded at 15,000 cells per well in 24-well plates, followed by lipofectamine LTX Plus transfection per manufacturer's protocol.

Immunoblotting

Cultured cells were washed in cold phosphate-buffered saline (PBS) and harvested on ice with lysis buffer (50 mM HEPES, 150 mM NaCl, 10% glycerol, 1 mM EDTA, 1% Triton X-100, 0.2% SDS) plus protease inhibitor cocktail (Roche; 11836170001) and phosphatase inhibitors (0.2 mM sodium orthovanadate, 1 mM sodium pyrophosphate). Protein concentration was determined by bicinchoninic acid (BCA) assay and equal protein amounts resolved on SDS–PAGE gels and electrotransferred to polyvinylidine fluoride membrane. Membrane was blocked with 5% bovine serum albumin (BSA) in Tris-buffered saline (TBS) tween 20 (TBST 0.1%) for 1–3 h and probed with primary antibodies: c-Myc (Life Technologies; 132500), FLAG (Sigma; M2, F3165), TRBP (Abcam; ab72110, or Proteintech; 15753-1-AP), Phospho-TRBP (custom), Hsc70 (Santa Cruz; sc7298), GST (Pierce; PA1-982A), and Lin28a (Cell Signaling; A177 3978S). All immunoblots were scanned and quantified without image adjustment. For representative image figures, image levels were uniformly and minimally adjusted for visual clarity in some instances.

Protein purification

GST-tagged proteins were purified from BL21 *Escherichia coli* using glutathione sepharose resin (GE Healthcare) according to the manufacturer's protocol, eluted with 10 mM glutathione at pH 7.4, and dialyzed to remove glutathione. MBP-Lin28a was purified using amylose resin (New England Biolabs) and MBP was cleaved with Factor XA (New England Biolabs) according to the manufacturer's protocols. In vitro pull down was carried out by binding GST proteins equimolar to 50 µg GST-TRBP-B overnight to glutathione resin, blocking with 5% BSA in PBS, then mixing with 25 µg purified Lin28a and rotated for 3 h at 4°C in PBS. The mixture was washed with 20× bead volume and then eluted by boiling in SDS gel loading buffer.

Immunoprecipitation

For FL-Lin28a coimmunoprecipitation of TRBP and its truncations, mouse anti-flag M2 antibody (Sigma) was adhered to protein G sepharose beads overnight after blocking with 5% BSA for 1 h. HEK 293T cells coexpressing the constructs of interest were harvested in coIP lysis buffer (100 mM KCl, 4 mM $MgCl_2$, 10 mM HEPES [pH 7.3], 50 µM $ZnCl_2$, 0.5% NP-40) with protease inhibitor cocktail (Roche), and phosphatase inhibitors (Sigma; phosphatase inhibitor cocktail 2 and 3). Insoluble material was first removed by centrifugation (10,000 × *g*) and lysates precleared by rotation (4°C, 1 h) with

unblocked sepharose beads. Equal masses of protein in precleared lysates were brought to equal volume, added to flag antibody-coated beads, and rotated (4°C, 3–4 h). After three washes with coIP wash buffer (150 mM NaCl, 1 mM $MgCl_2$, 50 mM HEPES [pH 7.8], 50 μM $ZnCl_2$, 0.05% NP-40), immunoprecipitated material was eluted at room temperature using 1× flag peptide (Sigma; F3290) diluted in coIP wash buffer.

Epifluorescence imaging

Live cell fluorescence and FRET imaging were conducted on a Zeiss Axiovert 200M microscope controlled by MetaFluor 6.2 software. Cells seeded on poly(L)lysine-coated glass-bottom imaging dishes (MatTek Corporation) were incubated at 37°C in Hank's balanced salt solution (HBSS) and imaged at 40× magnification with 50% neutral density filters, illuminated by an arc lamp and captured on a cooled charge coupled device (Photometrics). Fluorescence emission was collected from cyan fluorescent protein (420DF20 excitation filter, 500 ms excitation, 475DF40 emission filter); yellow fluorescent protein (420DF20 excitation for 50 ms, 535df25 emission filter); sensitized YFP emission (CFP excitation and YFP emission); and red fluorescent protein (568DF55 excitation filter, 50 ms, 600DRLP dichroic mirror, 653DF95 emission filter). For Figure 4H only, FRET efficiency imaging was conducted on an Olympus IX71 microscope controlled by MetaMorph software and illuminated by a pE300 LED light source (CoolLED) at 40× magnification.

For endpoint FRET imaging, cells expressing CFP-tagged TRBP or a truncation and YFP-tagged lin28a or a truncation were serum starved for approximately 15 min in imaging media. Several images were taken to establish a baseline, followed by 90 s, 3 min, and 5 min illumination at 504 nm to bleach YFP. Images were quantified using MetaFluor 6.2 software (Universal Imaging). FRET efficiency was calculated based on the recovery in background-corrected CFP brightness after YFP bleaching, using the formula FRET efficiency = $1 - F_{da}/F_d$ where F_{da} is the CFP fluorescence observed when both donor and acceptor are active and F_d is the fluorescence observed after YFP photobleaching. To confirm complete photobleaching, percent change in YFP intensity was calculated, using the formula

$$\%\ \text{photobleaching} = [(\text{intensity final} - \text{intensity initial})/\text{intensity initial}]*100\%$$

Only dishes with an average reduction of 80% or more in YFP signal were used for FRET efficiency calculation in epifluorescence experiments.

For time-course FRET imaging, cells expressing CFP-tagged TRBP-B with YFP-tagged Lin28a-3 were serum starved (0.5–2 h) in imaging media, then imaged every 30 s. CYFRET, CFP, YFP, and RFP intensity in each region of interest (ROI) were measured over time using MetaFluor software and, after background subtraction, used to calculate the normalized FRET emission ratio, a measure that adjusts for expression level and spectral bleedthrough of donor and acceptor fluorophores (Xia and Liu, 2001):

$$\text{NFRET} = \text{FRET intensity} - [\text{YFP intensity} \times a] - [\text{CFP intensity} \times b]$$
$$\text{NFRET ratio} = \text{NFRET/CFP}$$

Bleedthrough value "*a*" was determined using cells expressing only YFP and then imaged in both the CYFRET and YFP channels. "*a*" was defined as the signal in the YFRET channel as a percent of YFP signal; on this system, the value used was 0.14. Bleedthrough value "*b*" was calculated using the same approach with CFP alone, and came to 0.32. Representative images shown in Figure 5D have had the NFRET value calculated using the Image Calculator function in ImageJ to perform the same series of calculations (i.e., mean background subtraction in each channel, followed by subtraction of estimated bleedthrough from CFP and YFP direct channels, applied to CYFRET channel).

Statistical analyses

All quantified data represent mean ± SEM. Statistical analysis included one-way ANOVA for independent samples with a Bonferroni post hoc test, $\alpha = 0.05$, comparing with Lin28a alone or a comparable condition. Where noted, two-tailed Student's *t* tests were used for pairwise comparison of untreated and treated conditions (Figure 2, C and F). Linear regression analysis and slope significance testing were carried out using a Graphpad Prism protocol equivalent to ANCOVA. Before linear regression was performed, independent variables were subjected to a Grubb's test with $\alpha = 0.05$. The result was used to justify removing one statistically significant outlier from TRBP-full regression analysis (Figure 1H).

ACKNOWLEDGMENTS

We acknowledge the laboratory of Anne Gatignol and Aïcha Daher for TRBP truncation constructs and TRBP KO TEFs, Takanari Inoue for use of a fluorescence imaging system, Alexandra Amen for assistance with experimental troubleshooting and stimulating discussions, Sohum Mehta for imaging and data-handling assistance, and Timothy Gamache for assistance with purified proteins. This work was supported by the Braude Foundation, by National Institutes of Health (NIH) MH-098016 and MH-109341 (to M.K.M.), by NIH GM-111665 (to J.Z.), by NIH T32 GM-007445 (supporting L.O.), and by MH-084020 (to the Neuroscience Multiphoton Facility).

REFERENCES

Amen AM, Ruiz-Garzon CR, Shi J, Subramanian M, Pham DL, Meffert MK (2017). A rapid induction mechanism for Lin28a in trophic responses. Mol Cell 65, 490.

Baek D, Villen J, Shin C, Camargo FD, Gygi SP, Bartel DP (2008). The impact of microRNAs on protein output. Nature 455, 64–71.

Chen C, Zhu C, Huang J, Zhao X, Deng R, Zhang H, Dou J, Chen Q, Xu M, Yuan H, *et al.* (2015). SUMOylation of TARBP2 regulates miRNA/siRNA efficiency. Nat Commun 6, 8899.

Cho J, Chang H, Kwon SC, Kim B, Kim Y, Choe J, Ha M, Kim YK, Kim VN (2012). LIN28A is a suppressor of ER-associated translation in embryonic stem cells. Cell 151, 765–777.

Cousin C, Derouiche A, Shi L, Pagot Y, Poncet S, Mijakovic I (2013). Protein-serine/threonine/tyrosine kinases in bacterial signaling and regulation. FEMS Microbiol Lett 346, 11–19.

Daher A, Laraki G, Singh M, Melendez-Pena CE, Bannwarth S, Peters AH, Meurs EF, Braun RE, Patel RC, Gatignol A (2009). TRBP control of PACT-induced phosphorylation of protein kinase R is reversed by stress. Mol Cell Biol 29, 254–265.

Daher A, Longuet M, Dorin D, Bois F, Segeral E, Bannwarth S, Battisti PL, Purcell DF, Benarous R (2001). Two dimerization domains in the trans-activation response RNA-binding protein (TRBP) individually reverse the protein kinase R inhibition of HIV-1 long terminal repeat expression. J Biol Chem 276, 33899–33905.

Daniels SM, Melendez-Pena CE, Scarborough RJ, Daher A, Christensen HS, El Far M, Purcell DF, Laine S, Gatignol A (2009). Characterization of the TRBP domain required for dicer interaction and function in RNA interference. BMC Mol Biol 10, doi: 10.1186/1471-2199-10-38.

Ding Y, Li J, Enterina JR, Shen Y, Zhang I, Tewson PH, Mo GC, Zhang J, Quinn AM, Hughes TE, *et al.* (2015). Ratiometric biosensors based on dimerization-dependent fluorescent protein exchange. Nat Methods 12, 195–198.

Gonzalez F, Raden D, Davis R (1991). Identification of substrate recognition determinants for human Erk1 and Erk2 protein kinases. J Biol Chem 266, 22159–22163.

Griesbeck O, Baird G, Campbell R, Zacharias D, Tsien R (2001). Reducing the environmental sensitivity of yellow fluorescent protein—mechanism and applications. J Biol Chem 276, 29188–29194.
Huang YA, Ruiz CR, Eyler ECH, Lin K, Meffert MK (2012). Dual regulation of miRNA biogenesis generates target specificity in neurotrophin-induced protein synthesis. Cell 148, 933–946.
Jacobs D, Glossip D, Xing H, Muslin A, Kornfeld K (1999). Multiple docking sites on substrate proteins form a modular system that mediates recognition by ERK MAP kinase. Genes Dev 13, 163–175.
Jiang S, Baltimore D (2016). RNA-binding protein Lin28 in cancer and immunity. Cancer Lett 375, 108–113.
Kim Y, Yeo J, Lee JH, Cho J, Seo D, Kim JS, Kim VN (2014). Deletion of human tarbp2 reveals cellular microRNA targets and cell-cycle function of TRBP. Cell Rep 9, 1061–1074.
Kok KH, Ng M, Ching Y, Jin D (2007). TRBP and PACT directly interact with each other and associate with Dicer to facilitate the production of small interfering RNA. J Biol Chem 282, 17649–17657.
Laraki G, Clerzius G, Daher A, Melendez-Pena C, Daniels S, Gatignol A (2008). Interactions between the double-stranded RNA-binding proteins TRBP and PACT define the medipal domain that mediates protein-protein interactions. RNA Biol 5, 92–103.
Liu X, Chen M, Li L, Gong L, Zhou H, Gao D (2017). Extracellular signal-regulated kinases (ERKs) phosphorylate Lin28a protein to modulate P19 cell proliferation and differentiation. J Biol Chem 292, 3970–3976.
Llopis J, McCaffery M, Miyawaki A, Farquhart M, Tsien RY (1998). Measurement of cytosolic, mitochondrial, and golgi pH in single living cells with green fluorescent proteins. Proc Natl Acad Sci USA 95, 6803–6808.
Macek B, Mijakovic I (2011). Site-specific analysis of bacterial phosphoproteomes. Mol Cell Proteomics 11, 3002–3011.
Markwardt ML, Kremers G-J, Kraft CA, Ray K, Cranfill PJC, Wilson KA, Day RN, Wachter RM, Davidson MW, Rizzo MA (2011). An improved cerulean fluorescent protein with enhanced brightness and reduced reversible photoswitching. PLoS One 6, e17896.
Mayr F, Schuetz A, Doege N, Heinemann U (2012). The Lin28 cold-shock domain remodels pre-let-7 microRNA. Nucleic Acids Res 40, 7492–7506.
Miyawaki A (2011). Development of probes for cellular functions using fluorescent proteins and fluorescence resonance energy transfer. Annu Rev Biochem 80, 357–373.
Nagai T, Ibata K, Park E, Kubota M, Mikoshiba K, Miyawaki A (2002). A variant of yellow fluorescent protein with fast and efficient maturation for cell-biological applications. Nat Biotechnol 20, 87–90.
Nagai T, Yamada S, Tominaga T, Ichikawa M, Miyawaki A (2004). Expanded dynamic range of fluorescent indicators for Ca^{2+} by circularly permuted yellow fluorescent proteins. Proc Natl Acad Sci USA 101, 10554–10559.
Nam Y, Chen C, Gregory RI, Chou JJ, Sliz P (2011). Molecular basis for interaction of let-7 MicroRNAs with Lin28. Cell 147, 1080–1091.
Paroo Z, Ye X, Chen S, Liu Q (2009). Phosphorylation of the human microRNA-generating complex mediates MAPK/Erk signaling. Cell 139, 112–122.
Pereira S, Goss L, Dworkin J (2011). Eukaryote-like serine/threonine kinases and phosphatases in bacteria. Microbiol Mol Biol Rev 75, 192–212.
Rizzo M, Springer G, Granada B, Piston D (2004). An improved cyan fluorescent protein variant useful for FRET. Nat Biotechnol 22, 445–449.
Romoser V, Hinkle P, Persechini A (1997). Detection in living cells of Ca^{2+}-dependent changes in the fluorescence emission of an indicator composed of two green fluorescent protein variants linked by a calmodulin-binding sequence—a new class of fluorescent indicators. J Biol Chem 272, 13270–13274.
Ruiz CR, Shi J, Meffert MK (2014). Transcript specificity in BDNF-regulated protein synthesis. Neuropharmacology 76, 657–663.
Rybak A, Fuchs H, Smirnova L, Brandt C, Pohl EE, Nitsch R, Wulczyn FG (2008). A feedback loop comprising *lin*-28 and *let*-7 controls pre-*let*-7 maturation during neural stem-cell commitment. Nat Cell Biol 10, 987–993.
Selbach M, Schwanhaeusser B, Thierfelder N, Fang Z, Khanin R, Rajewsky N (2008). Widespread changes in protein synthesis induced by microRNAs. Nature 455, 58–63.
Shinoda G, Shyh-Chang N, de Soysa TY, Zhu H, Seligson MT, Shah SP, Abo-Sido N, Yabuuchi A, Hagan JP, Gregory RI, *et al*. (2013). Fetal deficiency of Lin28 programs life-long aberrations in growth and glucose metabolism. Stem Cells 31, 1563–1573.
Shyh-Chang N, Daley GQ (2013). Lin28: primal regulator of growth and metabolism in stem cells. Cell Stem Cell 12, 395–406.
Shyh-Chang N, Zhu H, Yvanka de Soysa T, Shinoda G, Seligson MT, Tsanov KM, Nguyen L, Asara JM, Cantley LC, Daley GQ (2013). Lin28 enhances tissue repair by reprogramming cellular metabolism. Cell 155, 778–792.
Stalder L, Heusermann W, Sokol L, Trojer D, Wirz J, Hean J, Fritzsche A, Aeschimann F, Pfanzagel V, Basselet P, *et al*. (2013). The rough endoplasmic reticiulum is a central nucleation site of siRNA-mediated RNA silencing. EMBO J 32, 1115–1127.
Tsanov KM, Pearson DS, Wu Z, Han A, Triboulet R, Seligson MT, Powers JT, Osborne JK, Kane S, Gygi SP, *et al*. (2017). LIN28 phosphorylation by MAPK/ERK couples signalling to the post-transcriptional control of pluripotency. Nat Cell Biol 19, 60–67.
Viswanathan SR, Powers JT, Einhorn W, Hoshida Y, Ng TL, Toffanin S, O'Sullivan M, Lu M, Phillips LA, Lockhart VL, *et al*. (2009). Lin28 promotes transformation and is associated with advanced human malignancies. Nat Genet 41, 843.
Warner MJ, Bridge KS, Hewitson JP, Hodgkinson MR, Heyam A, Massa BC, Haslam JC, Chatzifrangkeskou M, Evans G, Plevin MJ, *et al*. (2016). S6K2-mediated regulation of TRBP as a determinant of miRNA expression in human primary lymphatic endothelial cells. Nucleic Acids Res 44, 9942–9955.
Wilson RC, Tambe A, Kidwell MA, Noland CL, Schneider CP, Doudna JA (2015). Dicer-TRBP complex formation ensures accurate mammalian MicroRNA biogenesis. Mol Cell 57, 397–407.
Xia Z, Liu Y (2001). Reliable and global measurement of fluorescence resonance energy transfer using fluorescence microscopes. Biophys J 81, 2395–2402.
Zhou X, Clister TL, Lowry PR, Seldin MM, Wong GW, Zhang J (2015). Dynamic visualization of mTORC1 activity in living cells. Cell Rep 10, 1767–1777.
Zhu H, Shah S, Shyh-Chang N, Shinoda G, Einhorn WS, Viswanathan SR, Takeuchi A, Grasseman C, Rinn JL, Lopez MF, *et al*. (2010). Lin28a transgenic mice manifest size and puberty phenotypes identified in human genetic association studies. Nat Genet 42, 626–630.
Zhu H, Shyh-Chang N, Segre AV, Shinoda G, Shah SP, Einhorn WS, Takeuchi A, Engreitz JM, Hagan JP, Kharas MG, *et al*. (2011). The Lin28/let-7 axis regulates glucose metabolism. Cell 147, 81–94.